Study of the Initial Formation Stages of the Mesoporous Material SBA-15 Using Spin-Labeled Block Co-polymer Templates

Sharon Ruthstein,[†] Veronica Frydman,[‡] and Daniella Goldfarb*,[†]

Department of Chemical Physics and Chemical Research Support Unit, Weizmann Institute of Science, Rehovot 76100, Israel

Received: February 26, 2004; In Final Form: April 21, 2004

The hexagonal, silica-based, mesoporous material SBA-15 is prepared using poly(ethylene oxide)−poly(propylene oxide)−poly(ethylene oxide) block co-polymer (Pluronic P123, PEO_{20}−PPO_{70}−PEO_{20}) as a template and tetramethyl orthosilicate (TMOS) as a silica source. This work focuses on the investigation of its formation on the molecular level, with emphasis on the early stages of the reaction, when the interaction between silica precursors and the Pluronic micelles occurs. This was achieved using in situ X-band electron paramagnetic resonance (EPR) spectroscopy, in combination with electron spin−echo envelope modulation (ESEEM) experiments of Pluronic spin probes with different PEO and PPO chain lengths. In these Pluronic spin probes, the nitroxide spin label is located at the end of the PEO chain, which places them at different regions of the micelles. In the Pluronic micelles, the PPO chains define a hydrophobic region that is referenced as the core, whereas the more-hydrophilic PEO chains form the corona region. In the ESEEM experiments, the reaction was conducted in D_2O and it was quenched at different times by rapid freezing to 77 K. The ^2H modulation depth ($k(^2H)$) was followed, as a function of the reaction time. Four different systems, which were designed to probe the evolution of the reaction at three different regions of the Pluronic micelles, were examined. By comparing the ESEEM results with the in situ continuous wave (CW) EPR measurements of the different spin probes, four stages were detected. The first occurs within the first 5 min and is characterized by a large increase in the D_2O/OD density in the vicinity of all spin probes used, whether located in the core, the core/corona interface, or the corona/water interface. This was attributed to fast hydrolysis of the TMOS where hydrolyzed TMOS and water penetrate into the corona from the original location of the hydrophobic TMOS within the core. The second stage, which lasts ∼1 h, is characterized by a moderate reduction in the D_2O/OD density at the core/corona interface, attributed to silica polymerization. During the third stage (∼1 h), the D_2O/OD density decrease continues but is felt mainly in the corona region. The results show that the silica polymerization propagates outward from the core/corona interface.

Introduction

SBA-15 is a mesoporous material with a hexagonal arrangement of channels with diameters in the range of 2−30 nm. It benefits from a high hydrothermal stability and has relatively thick silica walls with a network of micropores[1−4] in addition to the well-ordered mesopores. It is synthesized with the nonionic poly(ethylene oxide)−poly(propylene oxide)−poly(ethylene oxide) block co-polymer (Pluronic P123, PEO_{20}−PPO_{70}−PEO_{20}).[4,5] This block co-polymer consists of a central hydrophobic PPO block, sandwiched between two hydrophilic PEO blocks, forming micelles in aqueous solutions. The micelles comprise a hydrophobic PPO core and a hydrophilic corona of hydrated PEO segments.[6−8] Block co-polymers have an advantage in that various micellar structures can be tuned by adjusting the solvent composition, molecular weight, or co-polymer architecture. Moreover, at low solution concentrations, they permit the organization of structures larger than those which can possibly be obtained with low-molecular-weight surfactants.[9] The presence of micelles in the Pluronic solution has been shown to be a prerequisite for the formation of SBA-15, and a correlation was observed between the critical micelle concentrations (CMCs) and the pore sizes.[4,10]

The interaction between the self-assembled template structure and the inorganic precursors, which provides the driving force for the formation of the long-range structural order, has been investigated in several ways, as reviewed by Ying et al.[11] and Patarin et al.[12] The majority of the mechanistic studies have concentrated primarily on the formation of MCM-41 with charged surfactants,[13−21] starting with Beck et al.,[22] who formulated the liquid-crystal templating (LCT) mechanism early after the discovery of the M41S materials. The introduction of appropriate spin probes into the reaction mixture allows the in situ electron paramagnetic resonance (EPR) investigation of the formation of the mesoporous materials on the molecular level.[23−26] In such experiments, one can probe changes in the polarity of the close environment of the spin label through changes in the ^{14}N hyperfine coupling (a_N).[27,28] Changes in the motional characteristics of the surfactant molecules can be followed by line-shape variations, induced by changes in the spin-probe mobility exerted by the forming silica.[23,24] In addition to in situ EPR experiments, the reaction can be investigated by electron spin−echo envelope modulation (ESEEM) experiments. This method provides information on the close environment of

* Author to whom correspondence should be addressed. Telephone: 972-8-934-3918. Fax: 972-8-934-4123. E-mail address: daniella.goldfarb@weizmann.ac.il.

[†] Department of Chemical Physics.

[‡] Chemical Research Support Unit.

10.1021/jp049133n CCC: $27.50
Published on Web 06/02/2004

the spin label,[29−32] through the detection of anisotropic hyperfine interactions between the unpaired electron and nearby nuclear spins, manifested as modulation in the echo decay.[33] The modulation depth parameter (k) is proportional to the electron−nuclear distance and the number of the nuclei around the unpaired electron.[33] Kevan and co-workers have extensively applied ESEEM methods to study photoionization and charge separation in micelles and vesicles.[34−37]

The ESEEM technique has been recently used to follow changes that occur in the packing and immediate environment of the surfactant molecules during room temperature formation of MCM-41.[38] This was done by introducing minute amounts of surfactant-like spin probes to the MCM-41 reaction mixture and quenching the mixture to liquid N_2 temperatures at different reaction times. In these experiments, the nuclear modulation was induced by ^{2}H nuclei of specifically deuterated surfactants, such as $\alpha-d_2-$CTAB (cetyl-trimethylammonium bromide). Alternatively, measurements that were conducted in D_2O detected changes in the water content of the surfactant/water interface region.

In a recent study, we investigated the formation mechanism of the mesoporous material SBA-15.[27] In this material, the source of the microporosity has been ascribed to PEO chains that are trapped within the silica region during the synthesis and are removed by calcination,[39] leaving open micropores. The spin probe used in this EPR study was L62-NO, which is a block co-polymer (Pluronic L62, $PEO_6-PPO_{30}-PEO_6$), with a nitroxide spin label replacing the −OH group at the end of the chain. The partition of L62-NO between the mesopores and micropores in as-synthesized SBA-15 could be readily detected through changes in the spectra, because of different motional characteristics.[27] It was found that, in aqueous micellar solutions of P123, the nitroxide of L62-NO is located within the micelles, close to the corona/core interface, whereas in L64 micelles ($PEO_{13}-PPO_{30}-PEO_{13}$), it is located close to the center of the corona. In the P123 synthesis, a partition of the L62-NO spin labels between two different environments was detected already after 20 min. One type of spin labels, with EPR spectra remaining invariant throughout the course of the synthesis, was assigned to the region of the silica network formation that penetrates into the corona. The changes in the local polarity of the environment of the other type of spin labels were attributed to their location at the corona/core interface, which undergoes a reduction of polarity during the first 2 h of the reaction.

In the present study, we have sought further insight into the formation of SBA-15, in particular, at the early stages of the reaction, when the interaction between the silica precursors and the surfactant assemblies occurs. This was done by the ESEEM technique, using L62-NO and 4-hydroxy-tempo-benzoate (4HTB) to probe different environments in the Pluronic micelles. The latter spin probe (4HTB) is hydrophobic and locates itself at the hydrophobic core of the micelles.[27] In addition, continuous wave (CW) EPR experiments were performed with two different Pluronic spin probes, P123−NO ($PEO_{20}-PPO_{70}-PEO_{20}$) and F127−NO ($PEO_{106}-PPO_{70}-PEO_{106}$), which have longer PEO segments and, therefore, probe regions closer to the water/corona interface and extend farther into the silica layer.

Experimental Section

Synthesis. The reagents used for the synthesis were as follows: Pluronic P123 ($PEO_{20}-PPO_{70}-PEO_{20}$, average molecular weight (M_{av}) of 5800), which was a gift from BASF Corp. (USA); Pluronic L64 ($PEO_{13}-PPO_{30}-PEO_{13}$, M_{av} = 2900) which was obtained from Aldrich; tetramethoxy orthosilane ($(CH_3O)_4Si$, TMOS; 98% pure, Merck), orthophosphoric acid (85% H_3PO_4, Fluka) and 4-hydroxy-tempo-benzoate (4HTB, Aldrich). The spin probes L62-NO, P123-NO, and F127-NO were synthesized as described in the literature.[40]

SBA-15 was synthesized according to the procedure reported by Zhao et al.,[41] except for the addition of the spin probe and the replacement of hydrochloric acid (HCl) by orthophosphoric acid (H_3PO_4).[27] A typical SBA-15 synthesis was as follows: to a 16 mL aqueous solution at 50 °C containing 0.5 g P123 (86.2 μmol) was added 20 μmol of the spin probe (L62-NO or others) and the mixture was stirred for a few minutes until the spin probe was dissolved. Then, 1.2 mL (12 mmol) of H_3PO_4 (85%) was added and the mixture was stirred for two more minutes, followed by the addition of 0.8 mL (5 mmol) of TMOS. The resulting mixture was left under stirring conditions for 20 h at 50 °C. Half of the gel solution was then filtered and dried at ambient temperature, and the other half was transferred into a Teflon bottle and heated at 100 °C for 24 h without stirring. After cooling to room temperature, the solid product was recovered by filtration, washed with distilled water and dried in air at ambient temperature. A typical molar composition of the synthesis gel was as follows: TMOS:1.7×10^{-2}P123:$2.4H_3PO_4$:$175D_2O$:4×10^{-3} spin probe (Si/P123 molar ratio of 59). SBA material was also synthesized with L64, using the same procedure, and the composition of the synthesis gel was as follows: TMOS:6.8×10^{-2}L64:$2.4H_3PO_4$:$175D_2O$:4×10^{-3} spin probe. The final product was characterized by small-angle X-ray (SAX) diffraction, using a diffractometer equipped with a Franks mirror and a one-dimensional position-sensitive detector (homemade), using nickel-filtered Cu Kα radiation (λ = 1.54 Å).[42] All final products exhibited SAX patterns that are typical of well-ordered SBA-15.[27]

Spectroscopic Measurements. EPR spectra were recorded on a Varian E-12 spectrometer that operated at a frequency of 9−9.5 GHz. Liquid samples were measured in flat cells. ESEEM experiments were performed on a home-built pulsed EPR spectrometer (9 GHz)[43] and a Bruker model E-580 spectrometer at 9.5 GHz, using quartz tubes with an outer diameter (OD) of 3 mm. The three-pulse ESEEM sequence, $\pi/2 - \tau - \pi/2 - T - \pi/2 - \tau -$ echo, was used with a four-step phase cycling.[44] The $\pi/2$ pulse length was 20 ns, and τ was set to 250 ns. The modulation depth is defined as $k = a/(a + b)$, where $a + b$ is the interpolated echo intensity between the first and second maxima and b is the echo intensity at the first minimum (see Figure 2 later in this work).

Results

ESEEM Experiments. ESEEM experiments on the reaction mixture cannot be performed in situ as in CW EPR measurements, because they must be conducted at low temperatures to slow the echo decay and to eliminate averaging of hyperfine anisotropy by motion. Therefore, the experiments were performed on reaction mixtures that were quenched by rapid freezing in liquid nitrogen at different reaction times. It has been already shown that, when such a rapid freezing occurs, the micellar structure is at least partially preserved.[38,45] In our experiments, the reaction was conducted in D_2O and the ^{2}H modulation depth ($k(^2H)$) was followed as a function of the reaction time. Because the magnitude of $k(^2H)$ is determined both by the number of ^{2}H nuclei and their distance from the unpaired electron,[33] in the following paragraphs, we shall refer to $k(^2H)$ as a measure for ^{2}H density. Time t = 0 min is the time before the addition of TMOS to the acidic micellar solution. To ensure effective mixing, the shortest measuring time was

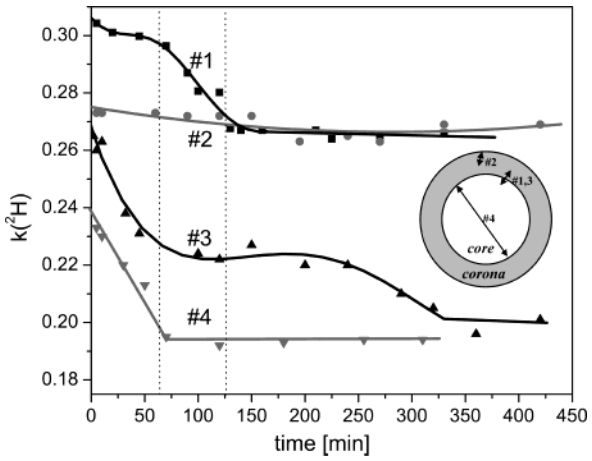

Figure 1. Time evolution of $k(^2H)$ for system 1 (L62-NO in the SBA-15 (Si/P123 = 59) reaction), system 2 (L62-NO in the SBA(L64) reaction), system 3 (L62-NO in the SBA-15 (Si/P123 = 118) reaction), and system 4 (4HTB in the SBA-15 (Si/P123 = 59) reaction). (The dotted vertical lines correspond to times of 60 and 130 min, and the solid lines have been drawn to guide the eye.) A schematic representation of the micelle shows the location range of the nitroxide label in the micelle for each system.

set to $t = 5$ min. Four different systems that allowed us to examine the evolution of the reaction at three different regions in the micelles were investigated:

(1) L62-NO in SBA-15 (Si/P123 = 59) for the core/corona interface.

(2) L62-NO in SBA(L64) for the corona region.

(3) L62-NO in SBA-15 (Si/P123 = 118) for the core/corona interface.

(4) 4HTB in SBA-15 (Si/P123 = 59) for the core region.

In an earlier work, the location of L62-NO and 4HTB within the micelles of L64 and P123 was determined by ESEEM spectroscopy.[27] In P123, L62-NO is situated at the corona/core interface region, whereas in L64, it is closer to the corona/water interface. On the other hand, 4HTB is situated at the hydrophobic core in both L64 and P123 micelles, because of its hydrophobic character (see scheme in Figure 1). Accordingly, systems 4, 1, and 2 were designed to explore the core region, the core/corona interface, and the corona region, close to the water interface, respectively. Systems 1 and 3 differ in the Si/Pluronic ratio, where the higher silicon content leads to a larger silica network and higher microporosity.[46,47]

The time evolution of $k(^2H)$ for all four systems for $t \geq 5$ min is presented in Figure 1. In system 1, $k(^2H)$ decreases gradually during the first 60 min, then a faster decay is observed for the next 60 min, after which it stabilizes at $k(^2H) = 0.26$. The reduction in $k(^2H)$ indicates a decrease in the ^2H nuclei (D_2O or OD) density in the vicinity of the nitroxide spin label. The time course of $k(^2H)$ in the SBA-15 system is consistent with the in situ CW EPR experiments that were performed earlier, showing a reduction in the polarity of the environment of the spin label located at the core/corona interface with a similar time dependence.[27] In system 2, $k(^2H)$ remains constant throughout the reaction; namely, there is no decrease in the ^2H density in the vicinity of the spin probe. This invariance is attributed to the location of the nitroxide label in the L64 micelles close to the corona/water interface, where the penetration of the silicate monomers/oligomers is not associated with polarity changes. This result is again consistent with earlier in situ EPR measurements, which did not reveal any change in the hyperfine coupling a_N during the reaction.[27] In contrast, 4HTB in system 4, which is located in the core region,

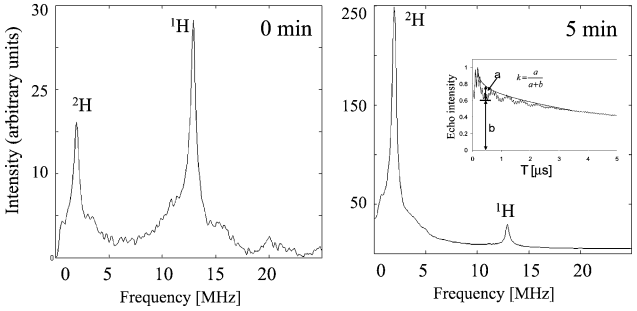

Figure 2. FT-ESEEM spectra of system 1 in D_2O sample before adding TMOS ($t = 0$ min) and 5 min after adding TMOS ($t = 5$ min). Inset shows the corresponding time domain trace and the definition of the modulation depth.

TABLE 1: Modulation Depth of the Different Systems at $t = 0$ min and $t = 5$ min

system number	Depth	
	$t = 0$ min	$t = 5$ min
1	0.07	0.30
2	0.09	0.28
3	0.07	0.27
4	0.03	0.23

experiences a significant decrease in $k(^2H)$ during the first 60 min of the reaction, after which it stabilizes at $k(^2H) \simeq 0.19$. This final value is lower than the final values measured in other systems. Finally, system 3 shows an initial fast decrease that lasts ~60 min. This decay is followed by a slower decay up to ~5 h, after which $k(^2H)$ stabilizes at ~0.2. After the samples were filtered and dried, $k(^2H)$ decreased to almost zero in all four systems.

Surprisingly, a considerable increase in $k(^2H)$ at $t = 5$ min, compared to $k(^2H)$ at $t = 0$ min, was observed for all systems investigated (see Table 1). The increase is observed very clearly in the Fourier-transformed spectra of the ESEEM traces, presented in Figure 2 for system 1. The addition of TMOS leads to a 13-fold increase in the relative intensities of the ^2H peak, compared to the ^1H peak.[48] The ^2H peak reflects the density of the exchangeable protons (water/OH/H^+ groups), whereas the ^1H signal represents protons of the polymer (the spin probe and TMOS (or generated methanol)). There could be several explanations for this increase: (1) The presence of hydrolyzed TMOS species such as $Si(OD)_{4-x}(OD_2)_x^{+x}$ and/or smaller oligomers, which may also carry significant amounts of D_2O molecules into the corona region; (2) The destruction of the micelles, such that the spin probe goes into solution. In this case, the $k(^2H)$ value of L62-NO in D_2O is expected to be 0.22;[27] and finally, (3) The swelling of the micelles due to the solvation of TMOS in the core of the micelles may also expand the corona and make it more water-accessible.

To distinguish between these possibilities, we have studied the effect of TMOS addition at neutral pH on the micellization.

TMOS Effect on Micellization. The CMC of P123 exhibits an unusual temperature dependence: the CMC value decreases as temperature increases. For example, it is 4.5 wt % at 17 °C and 3×10^{-4} wt % at 43 °C.[7] The effect of temperature on the micellization of a 2.5 wt % aqueous solution of P123 and 5 wt % L64 was investigated earlier by EPR of L62-NO at low and neutral pH.[27] As the temperature of the solutions increased from 23 °C to 40 °C, a decrease of 1.0 G in a_N was observed and attributed to the monomer to micelle transition. The possibility that the addition of TMOS destroys the micelles was verified by similar measurements on a solution of L62-NO in P123

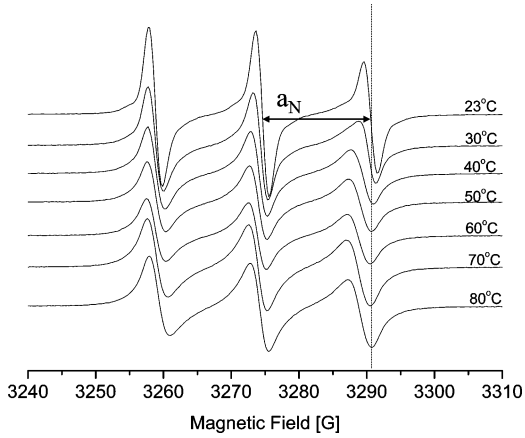

Figure 3. CW EPR spectra of L62-NO in a 2.5 wt % aqueous solution of P123 + TMOS (neutral pH) recorded at various temperatures. The vertical dotted line emphasizes the change in a_N and line width.

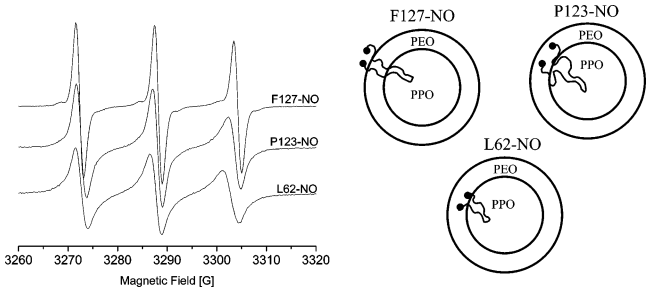

Figure 4. (Left) CW EPR spectra of L62-NO, P123-NO, and F127-NO in P123 micellar solutions at 50 °C. (Right) Schematic representations of the location of the spin probes in the micelles are also shown.

micelles with TMOS at neutral pH. At this pH, the hydrolysis of TMOS becomes increasingly slow (>200 min) and incomplete, whereas at pH < 2, the hydrolysis is fast and completed within <1 min.[49] The polymerization of the silicate monomers occurs simultaneously with hydrolysis and its rate increases at acidic or basic pH.[50] Figure 3 shows the temperature dependence of the EPR spectrum of 1mM L62-NO in a 2.5 wt % P123 aqueous solution with TMOS (Si/P123 = 59) at a neutral pH. The spectrum recorded at 23 °C shows a triplet with a_N = 16.1G, corresponding to L62-NO in water. At 40 °C, a_N decreased to 15.1G,[51] and no further changes were observed with an additional temperature increase. The observation of this transition, which is identical to that of a P123 solution without TMOS,[27] shows that the TMOS addition does not destroy the micelles.

ESEEM experiments also were performed on a P123 micellar solution with TMOS at neutral pH. Samples were taken from a solution that was kept at 50 °C at different times after the TMOS addition and were frozen as described previously. A sharp increase from $k(^2H) = 0.07$ to $k(^2H) = 0.2$ was observed; however, unlike in the acidic reaction mixture, the increase required 25 min, and then a thick silica gel was formed, preventing the transfer of a sample to the EPR tube. This indicates that it is the TMOS hydrolysis process which is responsible for the increase in the density of ^2H nuclei around the nitroxide label.

Other Pluronic Spin Probes. To gain more insight into the early stages of the reaction, we have examined the behavior of two additional spin probes, P123-NO and F127-NO, throughout the formation of SBA-15 with P123. Figure 4 presents the EPR spectra of L62-NO, P123-NO, and F127-NO in micellar solutions of P123 at 50 °C. F127-NO is characterized by the narrowest lines and the highest a_N value (a_N = 16.0G), which is almost comparable to that of the spin probe in water (a_N = 16.1G). This suggests that the location of F127-NO nitroxide is in the corona/water interface. L62-NO, which is located at the corona/core interface, has the lowest a_N value (a_N = 15.1G) and the broadest lines, whereas P123-NO with a_N = 15.3G is located at the corona of the micelles. The spectra of L62-NO, P123−NO, and F127-NO in as-synthesized dried SBA-15 prepared with Si/P123 = 59 (without the thermal stage) are compared in Figure 5. The spectrum of L62-NO is a superposition of a mobile species, attributed to the nitroxides in the mesopore region, and an immobilized species, assigned to spin labels trapped in the micropores.[27] The spectra of the other two spin probes show that the longer the PEO chain, the higher the relative amount of the immobilized species. The mobile species is completely absent for F127-NO 4-HTB in a P123 micellar solution and in the final dry solid SBA-15 product exhibit fast motion limit EPR spectra with the same hyperfine coupling (a_N = 15.0G), showing that, in both cases, it has no motional restrictions. This is expected, considering the size of 4-HTB and its location within the core region.

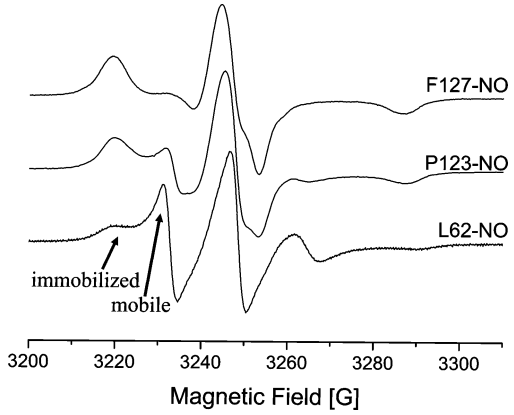

Figure 5. EPR spectra of L62-NO, P123-NO, and F127-NO in as-synthesized SBA-15 (Si/P123 = 59), recorded at room temperature.

The behavior of P123-NO in in situ CW EPR experiments was similar to that of L62-NO;[27] namely, a splitting in the high-field component of the triplet developed. The size of the splitting was larger than for L62-NO (results not shown). In contrast, the spectrum of F127-NO exhibited a single component throughout the reaction, with an a_N value of 16.0G, which is similar to the invariant component of the L62-NO spectra. This indicates that the F127-NO label is located entirely within the forming silica layer. However, the intensity of the signal exhibits a considerable decrease during the reaction, as shown in Figure 6. The intensity reduction is due to disproportionation of the nitroxide radical at low pH, resulting in a diamagnetic hydroxylamine. The disproportionation of nitroxides is reversible; however, at pH <2, the rate of the forward reaction is much higher than that of the reversed one.[52] Two steps can be clearly identified: a fast one that occurs at t < 5 min, followed by a milder decay that reaches a constant after ∼80 min. This decrease cannot be explained by a pH change, because the pH of the solution was constant throughout the reaction (pH = 1.3). Hence, we conclude that, during the early stages of the reaction, the spin label is exposed to acid attack; however, after the TMOS hydrolysis is complete and silicates start to polymerize within the corona region, it becomes protected and the disproportionation slows and eventually stops. In the absence of TMOS, the intensity of the signal of F127-NO in P123 micelles at the same pH decreases by 10%−15% during the first 10 min

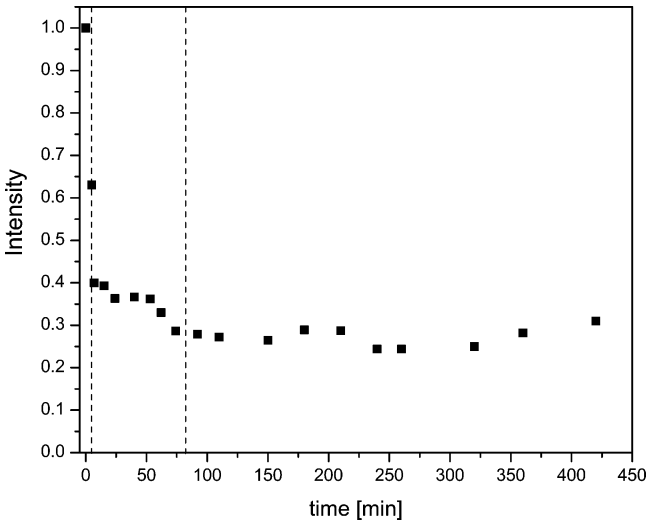

Figure 6. Normalized intensity of the CW EPR signal of F127-NO in the reaction mixture of SBA-15 (Si/P123 = 59), as a function of the reaction time. Dashed vertical lines correspond to reaction times of 5 and 80 min.

after the addition of acid. These results show that the addition of TMOS leads to an increase of $[H^+]$ in the corona region.

Discussion

The ESEEM and EPR results, obtained from the different spin probes that were added to the SBA-15 reaction mixture with Si/P123 = 59, indicate the presence of the four following stages: (a) Initially, at $t < 5$ min, there is a large increase in the D_2O/OD density in all regions of the micelles, and considerable decomposition of spin labels that are situated at the corona/water interface occurs; (b) During the period of $t = 5-60$ min, the spin labels located at the corona/water interface decompose at a milder rate and the D_2O/OD density in the core and core/corona interface decreases; (c) At $t = 60-120$ min, a further decrease of the D_2O/OD density in the core/corona interface is observed; and, finally, (d) For $t > 120$ min, no further changes in the local environment of the spin labels are detected. Stages (b)−(d) are marked on Figure 1.

Stage (a) involves the penetration of hydrophobic TMOS molecules ($Si(OCH_3)_4$) into the core of the micelles, with a simultaneous hydrolysis, leading to the introduction of water, methanol (CH_3OD), and hydrolyzed TMOS (monomers such as $Si(OD)_{4-x}(OD_2)_x^{x+}$) or partially hydrolyzed TMOS into the corona, causing an increase in the D_2O/OD density in all regions. Most of the methanol eventually evaporates (the temperature is 50 °C), whereas the silica monomers interact with the PEO in the corona via hydrogen bonds. The penetration of silicate monomers and water into the corona region could be mediated by the phosphate anions as suggested earlier,[4] although this has not yet been observed experimentally. The penetration of D_2O and silicate monomers all the way to the core/corona interface is evident from the increase of $k(^2H)$ measured for the system prepared with the 4HTB spin probe (system 4). Stage (b) is associated with the polymerization (condensation) of the $Si(OD)_{4-x}(OD_2)_x^{x+}$ monomers, which causes a reduction of the ^2H density at the corona/core interface. This was felt by the hydrophobic 4HTB spin probe, which is located throughout the core, but was barely sensed by the L62-NO spin probe that is located deeper in the corona region and toward the water interface. The reason for that is the extension of silica species into the core region, which causes the organic/inorganic interface to migrate outward, while the water generated by the condensation remains within the forming silica network. Evidence for this is the invariance of $k(^2H)$ in the L62-NO/L64 system and its narrow, fast-limit-type lineshapes in the CW EPR spectra. The fluid silica layer formed during stage (b) is already sufficient to protect F127-NO from the acidic attack. During stage (c), no further changes are sensed in the core region (4HTB), whereas a rapid reduction of $k(^2H)$ within the corona is still in progress. This can be explained by further condensation of the silica monomers and contraction of the silica network, associated with migration of the organic/inorganic interface outward from the corona region, which causes the depletion of water from this region. This suggests that the reaction progresses from the core toward the corona.

Unfortunately, the ESEEM technique can only probe changes in the local environment of the spin probe but it does not sense directly the establishment of any long-range order or changes in the shapes and sizes of the molecular assemblies. In EPR spectra, the lineshapes can, in principle, indicate the onset of an ordering potential, which is typical for liquid crystalline phases, if the resulting molecular motion is within the right dynamic range.[24] Similarly, slowing of the molecular motion can be attributed to an increase in size of the aggregates or to an association of micelles. In these cases, it should be possible to distinguish between local motions of the probe within the aggregate and global motion of the aggregate itself. Our in situ EPR measurements on the various spin probes reveal fast-motion-limit spectra throughout the entire reaction, indicating low ordering and a free motion of the ends of the PEO chains, where the nitroxide labels are located. This situation changes drastically upon drying, where the motion of the PEO end chains that are trapped within the silica region is within the rigid limit.[27] Our earlier X-ray diffraction (XRD) measurements,[27] involving drying of the samples after various reactions times, have shown that the hexagonal order of the SBA-15 structure is already formed after 2 h, which corresponds to stage (d). In the hexagonal phase, the effective volume of the polar head is smaller than that in the micelles. Hence, if we assume that the micelles in solution are spherical and not rodlike, a transition to rodlike micelles or a hexagonal structure should be associated with a contraction in the polar head region, and a decrease in the distances between neighboring molecules. If the polar head region is located at the core/corona interface, then such a contraction can occur via polymerization. Therefore, it is possible that stages (b) and/or (c) are associated with the formation of rodlike micelles, micelle aggregation, and the formation of hexagonal order.

Finally, with the help of the aforementioned model, the differences between systems 1 (Si/P123 = 59) and 3 (Si/P123 = 118) should be explained. In system 3, a precipitate is detected in the reaction solution already after 20 min, whereas for system 1, this occurs only after 45 min. This observation indicates that, for the sample with a high Si/P123 ratio, the polymerization is faster. This difference can be the reason for the moderate decay of $k(^2H)$ at the beginning of the reaction of SBA-15 (Si/P123 = 59) and the steeper change for system 3 during stage (b). Assuming that the silica layer in SBA-15 (Si/P123 = 118) is thicker, because of a higher silicon concentration,[46] it should require a longer condensation (cross-linking) time for the silica formation, and therefore, a longer time for the depletion of water from the corona region. This manifested itself in the ESEEM experiment by a significant longer stage (c). The lower $k(^2H)$ value of system 3 at $t = 5$ min, compared to system 1 (Table 1), is also attributed to a faster polymerization rate, such that a significant migration of water and hydrolyzed TMOS molecules

away from the core/corona interface has already occurred, leading to a lower value of $k(^2H)$.

Flodström et al.[53] recently reported an in situ ^1H NMR study of the formation of SBA-15, and the signals of the PPO methyls of P123 were followed, as a function of time. A gradual broadening was observed during the first 20 min, followed by a transition that took ~5 min, to a residual dipolar width of 1.5 kHz. The latter is also typical for the final product. This transition occurred together with the appearance of a precipitate. Hence, the changes in the linewidth were attributed to an increase of the micellar size, initially through an elongation of the micelles and followed by clustering of the micelles to form flocs and a precipitate that later transforms to the hexagonal structure. The clustering was attributed to the interaction of the PEO with the silica polymers, which reduces the repulsion between the micelles. This interpretation was based on transmission electron microscopy (TEM) micrographs obtained from samples, for which the reaction was first quenched by dilution and then retrieved by drying. Although these conditions are different from those under which the NMR measurements were conducted, especially the drying process, the authors believe that a qualitative correlation is nevertheless appropriate. The earliest stage observed in the NMR experiment, between 7 and 24 min from the TMOS addition, seems to correspond to our stages (b) and (c), and the faster rate is attributed to the use of HCl in the reaction, compared to H_3PO_4 in our case.[4]

There are two main issues that should be considered while comparing the results of the in situ NMR study with our in situ EPR results. When the motional averaging of molecular segments within a micelle is considered, one must consider the local motion of the segments, lateral diffusion, and the motion of the micelle as a whole. The tumbling rate of micelles with a size of 10 nm, such as our P123 micelles, is 10^{-6} s.[53] This rate is too slow to average the anisotropic hyperfine interaction of a nitroxide, which is on the order of 100 MHz. Thus, the observed motional averaging is a consequence of the local motion of the nitroxide groups. Hence, the EPR spectrum of the Pluronic spin probes is sensitive only to changes in the local motion that are caused by the silica polymerization, rather than to an increase in size of the aggregates or their clustering. Because the nitroxide labels are located at the ends of the PEO chains, they can, in principle, move in all directions and average almost completely their hyperfine anisotropy, as is indeed observed prior to drying. In contrast, the micellar tumbling is fast enough to average the dipolar interaction of the protons within a methyl group; therefore, a significant change in the aggregate size will have a considerable effect on the width of the NMR signal, provided that the local motion is hindered.[53] In the case of the protons of the PPO segments, as opposed to the ends of the PEO segments, the local motion is hindered and cannot lead to a fully averaged dipolar interaction. Hence, the information obtained from the two methods is complementary, and the NMR is sensitive mostly to the particle size, whereas the EPR is primarily sensitive to the local motion.

Figure 7 presents a schematic model that summarizes the initial steps of the formation mechanism of SBA-15, focusing on the process that occurs within the individual micelles, not considering changes in shape/length. Initially, the polymer chains are packed together and form micelles. After adding acid + TMOS to the micellar solution, TMOS and partially hydrolyzed TMOS, which are hydrophobic molecules, penetrate into the core (stage (a)). Hydrolysis occurs very fast and hydrolyzed monomers diffuse into the corona region, where the polymerization process of the silica begins, causing a depletion

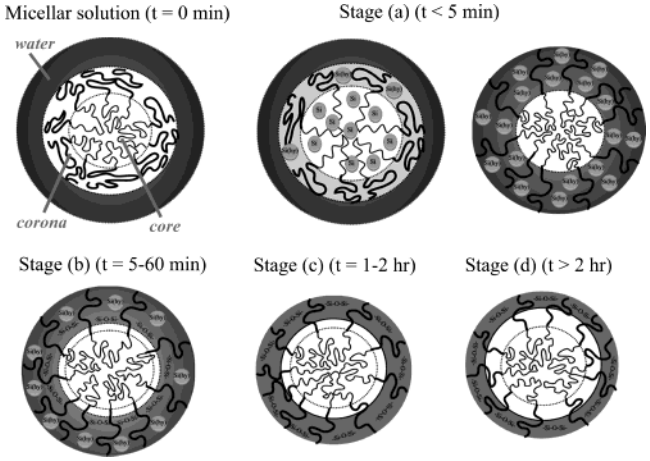

Figure 7. Proposed model for the initial stages in the formation of SBA-15 (Si/P123 = 59). Gray scale in the corona region represents the amount of D_2O/OD; dark gray denotes a large amount of water in the corona region, whereas light gray denotes a region with less water. Legend is as follows: Si ≡ $Si(OCH_3)$; Si(hy) ≡ $Si(OD)_{4-x}(OD_2)_x^{x+}$.

of D_2O/OD from the corona region and/or migration of forming silica network outward. During the first hour (stage (b)) of the reaction, this is felt at the core/corona interface and at the second hour (stage (c)) of the reaction in the corona region. Through comparison with the NMR results, stage (b) may also associated with lengthening of the micelles and stage (c) with clustering of the micelles resulting in larger aggregates[53] that precipitates.

While revising the manuscript, the results of a new in situ synchrotron SAXS/XRD study of the formation of SBA-15 were brought to our attention.[54] Although the synthesis was conducted under somewhat different conditions (a reaction temperature of 35 °C, and HCl was used, rather than H_3PO_4), the conclusions of this work are consistent with our model. It was found that the micelles are present up to 40 min and then a transition to a two-dimensional hexagonal structure occurs. Moreover, after the hexagonal order is formed, there is a continuous increase of the hydrophobic core and a decrease in the silica wall thickness, as described in our model at stages (b)−(d).

Conclusions

A proposed model for the initial steps of SBA-15 formation (Si/P123 molar ratio of 59) has been suggested, based on electron paramagnetic resonance (EPR) and electron spin-echo envelope modulation (ESEEM) experiments of different Pluronic spin probes. The reaction was shown to propagate from the core of the micelles into the corona/water interface. The fast hydrolysis of the tetramethoxy orthosilane (TMOS) is associated with a penetration of water, acid, and silica monomers into the corona region. As the polymerization begins, the D_2O/OD density decreases, starting from the core/corona interface into the corona/water region. For Si/P123 = 59, the reaction is completed in 2 h, whereas for higher silicon content, a longer time is required, although the initial stage is shorter.

Acknowledgment. This research was supported by the Center of Excellence, "Origin of Ordering and Functionality in Mesostructured Hybrid Materials". Supported by The Israel Science Foundation (under Grant No. 800301-1). The Gerhard M. J. Schmidt Minerva Center for Supramolecular Architecture (Minerva is funded through the BMBF) and the Ilse Katz Institute for Material Science and Magnetic Resonance Research are acknowledged for their kind support.

References and Notes

(1) Impèror-Clerc, M.; Davidson, P.; Davidson, A. *J. Am. Chem. Soc*. **2000**, *122*, 11925−11933.

(2) Ryoo, R.; Ko, C. H.; Kruk, M.; Antochshuk, V.; Jaroniec, M. *J. Phys. Chem. B* **2000**, *104*, 11465−11471.

(3) Kruk, M.; Jaroniec, M.; Joo, S. H.; Ryoo, R. *J. Phys. Chem. B* **2003**, *107*, 2205−2213.

(4) Zhao, D.; Huo, Q.; Feng, J.; Chmelka, B. F.; Stucky, G. D. *J. Am. Chem. Soc*. **1998**, *120*, 6024−6036.

(5) Zhao, D.; Feng, J.; Huo, Q.; Melosh, N.; Fredrickson, G.; Chmelka, B. F.; Stucky, G. D. *Science* **1998**, *279*, 548−552.

(6) Alexandridis, P.; Hatton, T. A. *Colloids Surf. A* **1995**, *96*, 1−46.

(7) Wanka, G.; Hoffmann, H.; Ulbricht, W. *Macromolecules* **1994**, *27*, 4145−4159.

(8) Guo, L.; Colby, R. H.; Lin, M. Y.; Dado, G. P. *J. Rheol. (N.Y.)* **2001**, *45*, 1223−1242.

(9) Förster, S. *Top. Curr. Chem.* **2003**, *226*, 1−28.

(10) Kipkemboi, P.; Fogden, A.; Alfredsson, V.; Flodstrom, K. *Langmuir* **2001**, *17*, 5398−5402.

(11) Ying, J. Y.; Mehnert, C. P.; Wong, M. S. *Angew. Chem., Ind. Ed*. **1999**, *38*, 56−77.

(12) Patarin, J.; Lebeau, B.; Zana, R. *Curr. Opin. Colloid Interface Sci*. **2002**, *7*, 107−115.

(13) Firouzi, A.; Kumar, D.; Bull, L. M.; Besier, T.; Sieger, P.; Huo, Q.; Walker, S. A.; Zasadzinski, J. A.; Glinka, C.; Nicol, J.; Margolese, D.; Stucky, G. D.; Chmelka, B. F. *Science* **1995**, *267*, 1138−1143.

(14) Frasch, J.; Lebeau, B.; Soulard, M.; Patarin, J.; Zana, R. *Langmuir* **2000**, *16*, 9049−9057.

(15) Huo, Q.; Margolese, D. I.; Ciesla, U.; Demuth, D. G.; Feng, P.; Gier, T. E.; Sieger, P.; Firuzi, A.; Chmelka, B. F.; Schüth, F.; Stucky, G. D. *Chem. Mater*. **1994**, *6*, 1176−1191.

(16) Tanev, P. T.; Pinnavaia, T. J. *Science* **1995**, *267*, 865−867.

(17) Bagshaw, S. A.; Prouzet, E.; Pinnavaia, T. J. *Science* **1995**, *269*, 1242−1244.

(18) Pevzner, S.; Regev, O. *Microporous Mesoporous Mater*. **2000**, *38*, 413−421.

(19) Pevzner, S.; Regev, O.; Lind, A.; Linden, M. *J. Am. Chem. Soc*. **2003**, *125*, 652−653.

(20) Linden, M.; Schunk, S. A.; Schüth, F. *Angew. Chem., Int. Ed*. **1998**, *37*, 821−823.

(21) Sadasivan, S.; Fowler, C. E.; Khushalani, D.; Mann, S. *Angew. Chem., Int. Ed*. **2002**, *41*, 2151−2153.

(22) Beck, J. S.; Vartuli, J. C.; Roth, W. J.; Leonowicz, M. E.; Kresge, C. T.; Schmidt, K. D.; Chu, C. T.-W.; Olson, D. H.; Sheppard, E. W.; McCullen, S. B.; Higgins, J. B.; Schlenker, J. L. *J. Am. Chem. Soc*. **1992**, *114*, 10834−10843.

(23) Zhang, J.; Luz, Z.; Goldfarb, D. *J. Phys. Chem.* **1997**, *101*, 7087−7094.

(24) Zhang, J.; Luz, Z.; Zimmermann, H.; Goldfarb, D. *J. Phys. Chem. B* **2000**, *104*, 279−285.

(25) Ottaviani, M. F.; Galarneau, A.; Desplantier-Giscard, D.; Renzo, F. D.; Fajula, F. *Microporous Mesoporous Mater*. **2001**, *44*−*45*, 1−8.

(26) Galarneau, A.; Renzo, F. D.; Fajula, F.; Mollo, L.; Fubini, B.; Ottaviani, M. F. *J. Colloid Interface Sci*. **1998**, *201*, 105−107.

(27) Ruthstein, S.; Frydman, V.; Kababya, S.; Landau, M.; Goldfarb, D. *J. Phys. Chem. B* **2003**, *107*, 1739−1748.

(28) Caldararu, H. *Spectrochem. Acta, Part A* **1998**, *54*, 2309−2336.

(29) Szajdzinska-Pietek, E.; Maldonado, R.; Kevan, L.; Jones, R. R. M.; Coleman, M. J. *J. Am. Chem. Soc*. **1985**, *107*, 784−788.

(30) Jones, R. R. M.; Maldonado, R.; Szajdzinska-Pietek, E.; Kevan, L. *J. Phys. Chem*. **1986**, *90*, 1126−1129.

(31) Szajdzinska-Pietek, E.; Maldonado, R.; Kevan, L.; Berr, S. S.; Jones, R. R. M. *J. Phys. Chem*. **1984**, *89*, 1547−1550.

(32) Baglioni, P.; Kevan, L. *J. Phys. Chem*. **1987**, *91*, 1516−1518.

(33) Kevan, L.; Schwartz, R. N. *Time Domain Electron Spin Resonance*; Wiley−Interscience: New York, 1979; Chapter 8.

(34) Kang, Y. S.; Kevan, L. *J. Phys. Chem*. **1994**, *98*, 7624−7627.

(35) Stenland, C.; Kevan, L. *Langmuir* **1994**, *10*, 1129−1133.

(36) Kurshev, V. V.; Kevan, L. *J. Phys. Chem*. **1995**, *99*, 10616−10620.

(37) Baglioni, P.; Rivara-Minten, E.; Kevan, L. *J. Phys. Chem.* **1988**, *92*, 4726−4730.

(38) Zhang, J.; Carl, P. J.; Zimmermann, H.; Goldfarb, D. *J. Phys. Chem. B* **2002**, *106*, 5382−5389.

(39) Kruk, M.; Jaroniec, M.; Ko, C. H.; Ryoo, R. *Chem. Mater*. **2000**, *12*, 1961−1968.

(40) Caragheorgheopol, A.; Caldararu, H.; Dragutan, I.; Joela, H.; Brown, W. *Langmuir* **1997**, *13*, 6912−6921.

(41) Zhao, D.; Sun, J.; Li, Q.; Stucky, G. D. *Chem. Mater.* **2000**, *12*, 275.

(42) Cheethman, J. J.; Wachtel, E.; Bach, D.; Epand, R. M. *Biochemistry* **1989**, *28*, 8928.

(43) Shane, J. J.; Gromov, I.; Vega, S.; Goldfarb, D. *Rev. Sci. Instrum*. **1998**, *69*, 3357.

(44) Fauth, J.-M.; Schweiger, A.; Braunschweiler, L.; Forrer, J.; Ernst, R. R. *J. Magn. Reson.* **1986**, *66*, 74−85.

(45) Ottaviani, M. F.; Daddi, R.; Brustolon, M.; Turro, N. J.; Tomalia, D. A. *Langmuir* **1999**, *15*, 1973−1980.

(46) Miyazawa, K.; Inagaki, S. *Chem. Commun*. **2000**, 2121−2122.

(47) Van De Voort, P.; Ravikovitch, P. I.; De Jong, K. P.; Neimark, A. V.; Janssen, A. H.; Benjelloun, M.; Van Bavel, E.; Cool, P.; Weckhuysen, B. M.; Vansant, E. F. *Chem. Commun*. **2002**, 1010−1011.

(48) We have looked for ^{31}P modulation but none of the sample showed a ^{31}P peak. Similarly, no ^{29}Si modulation was observed. However, the latter is expected, because of the low natural abundance of ^{29}Si.

(49) Aelion, R.; Loebel, A.; Eirich, F. *J. Am. Chem. Soc*. **1950**, *72*, 5705−5712.

(50) Iler, R. K. *The Chemistry of Silica*; Wiley: New York, 1979.

(51) The a_N value is 1.2G smaller than the values reported earlier, because of an instrumental problem in the earlier measurements.[27]

(52) Rozantsev, E. G. *Free Nitroxyl Radicals*; Plenum Press: New York, 1970.

(53) Flodström, K.; Wennerström, H.; Alfredsson, V. *Langmuir* **2004**, *20*, 680−688.

(54) Flodström, K.; Teixeira, C. V.; Amenitsch, H.; Alfredsson, V.; Lindén, M. In Situ Synchrotron Small-Angle X-ray Scattering/X-ray Diffraction Study of the Formation of SBA-15 Mesoporous Silica. *Langmuir*, in press.